IEEE Access
Multidisciplinary | Rapid Review | Open Access Journal

Received 8 February 2024, accepted 17 March 2024, date of publication 21 March 2024, date of current version 27 March 2024.

Digital Object Identifier 10.1109/ACCESS.2024.3380188

RESEARCH ARTICLE

A Bayesian Optimized Deep Learning Approach for Accurate State of Charge Estimation of Lithium Ion Batteries Used for Electric Vehicle Application

SELVARAJ VEDHANAYAKI AND VAIRAVASUNDARAM INDRAGANDHI
Vellore Institute of Technology, Vellore 632014, India

Corresponding author: Vairavasundaram Indragandhi (indragandhi.v@vit.ac.in)

This work was supported by the Royal Academy of Engineering, U.K., under Grant TSP-2325-5-IN_172.

ABSTRACT Battery technology used in Electric Vehicles has recently drawn numerous researchers' attention. Monitoring of battery condition, especially the state of charge, is necessary to ensure the safe and reliable operation of the battery. Even though researchers have proposed numerous SOC estimation techniques, exploration is still required to find a suitable technique that can adapt versatile lithium-ion battery chemistries. Deep learning (DL) is a well-known machine learning strategy that has been shown to outperform many other approaches for SOC estimation in recent studies. However, choosing the right hyperparameters and appropriate use of suitable input parameters is crucial to get the best performance out of DL models. Currently, researchers use well-established heuristics approaches to choose hyperparameters by manual tuning or using thorough search techniques like grid search and random search. This leads the models to be inefficient and less accurate. This paper suggests a methodical, automated procedure for choosing hyperparameters using a Bayesian optimisation algorithm. In addition to that, average voltage and average current are used as the important input parameters along with battery parameters (current, voltage and temperature) for accurate SOC prediction as they involve the past and present history of voltages and load conditions, respectively. The proposed methods are validated and tested for varying hidden neuron count with four different datasets involving different temperatures, namely, -10°C, 0°C, 10°C and 25°C. The findings demonstrate that, for all three RNN types (LSTM, GRU and BiLSTM), the ideal configuration yields SOC estimations with less than 2% root mean square and 5% maximum error. Among the three, BiLSTM with 70 hidden neurons estimates SOC with reduced estimation error compared to other methods. By utilizing the suggested approach, battery management systems that monitor the condition of batteries in various environmental circumstances can become more reliable.

INDEX TERMS Electric vehicle, battery management system, state of charge, long short term memory, gated recurrent unit, bilayer LSTM.

I. INTRODUCTION

Countries create energy-saving and emission-reduction technology to reduce carbon dioxide emissions and environmental repercussions like climate change, sea level rise, greenhouse effect, and biodiversity loss. COP26 in Glasgow, UK, addressed these energy crisis challenges. Government leaders from several countries, business people, and groups focused on 100% zero-emission vehicles met to develop principles to accomplish the Paris Agreement goals by 2040 [1]. In [2], the researcher states that car electrification and renewable energy sources are promising solutions to the energy crisis and 40% GHGE reduction. In 2021, EV sales reached 6.75 million units, up 108% from 2020, since they minimize car emissions and store renewable energy [3].

Current energy storage methods in transportation include lithium-ion, nickel-cobalt, lead acid, and nickel-cadmium batteries [4]. Lithium-ion batteries are preferred for their

The associate editor coordinating the review of this manuscript and approving it for publication was Giambattista Gruosso.

higher specific power, energy density, longevity, and lower self-discharge rate [5]. Lithium-ion batteries have NMC, NCA, LFP, LCO, LMO, and LTO chemical compositions. Li-ion battery characteristics are compared in Figure 1. The figure demonstrates that nickel cobalt aluminium oxide (NCA) batteries have the best specific energy and power. Reduced manufacturing cost is a key factor in Li-ion battery adoption across industries. Although Li-ion batteries have many benefits, they need a safe operating zone. Since Li-ion batteries use a charge transfer reaction to store energy, regular use of the battery causes problems with degradation. These problems include the loss of active materials and lithium inventory, the formation and breakdown of Solid Electrolyte Interface film, and a deposit of metallic lithium in the anode. Thus, exceeding lithium-ion battery packs' tolerance will damage them and make them dangerous [6]

A BMS is a software and hardware controller that improves battery life and performance. Figure 2 depicts BMS schematically. Estimating the State of Charge, State of Health, cell balance, charge and discharge control, and thermal and power flow management are essential battery management system activities. SOC estimate is crucial among all the functions [7]. SOC is defined as a ratio of the battery's remaining capacity to the rated capacity at a specific condition by the US Advanced Battery Consortium (USABC) [8].

Due to their unique diffusion method and complex electrochemical reaction, Li-ion batteries' rated capacity will not match the manufacturer's rating. The battery's rated capacity will also change with age, temperature, and environmental conditions. Along with manufacturing faults, potentiometric, amperometric, and conductometric sensor limitations affect SOC estimation [9]. Numerous methods, including the Open Circuit Voltage method, the Ampere Hour method, model-based methods, filter-based methods, observer-based methods, and data-based methods, have been presented for the purpose of providing an accurate assessment of voltage over current (SOC).

The estimation of SOC is critical in BMS. Because of their recursive nature, many articles proposing SOC estimates use Kalman filter-based algorithms [10], [11], [12]. The main disadvantage of Kalman filter-based approaches is that they necessitate precise battery modelling and parameter identification. Because ML approaches do not impose chemical or electrical models, they provide an alternative to precise SOC prediction in light of the significant challenges associated with battery modelling [13]. Most of the ML methods use SVM and ANN. However, these methods have certain limitations that reduce SOC estimating performance. The manual construction of characteristics from raw signal data at the input data level requires a lot of labour and skill. Despite their limited analytical capability and inability to handle high-dimensional data, shallow learning architectures are used at the model scale [14]. Through the use of multi-layer nonlinear transformations, deep learning has the potential to construct deep neural networks (DNNs), which possess the ability to hierarchically extract complicated

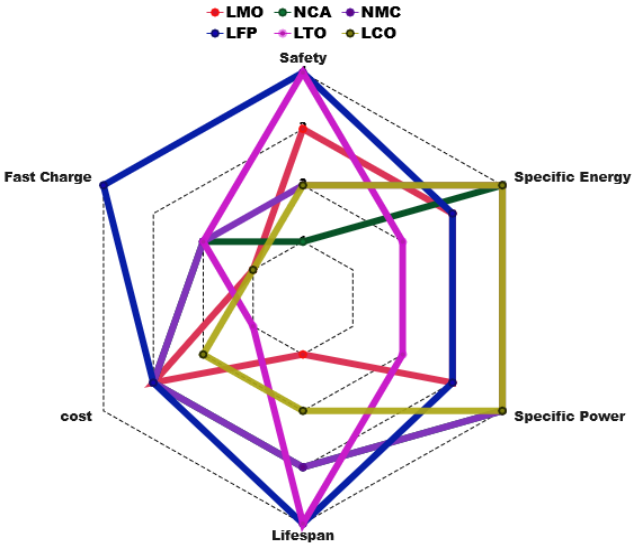

FIGURE 1. Application Comparison of lithium-ion batteries preferred for EV.

feature information from input data. In order to automatically extract the internal representation from the input signal and estimate LiB SOC, a DNN-based end-to-end estimator is able to perform automatically. Recent years have seen the development of a multitude of DNN-based SOC estimate approaches, including LSTM, GRU, and BiLSTM [15], [16], [17], [18]. A major advantage of RNN-based SOC estimate methods over conventional approaches is: No requirement for operating-characteristic battery models. Self-learning its weight and bias eliminate the need for hand engineering and parametrization.

One of the major concerns of the data-driven method is the selection of model hyperparameters, namely, learning rate, number of hidden units, hidden neurons, batch size, epochs, activation function and dropout rate. The inappropriate selection of hyperparameters leads to a reduction in prediction accuracy [19]. Researchers employ a trial-and-error approach for hyperparameter selection. Training computation demands make empirical hyperparameter selection for deep learning models time-consuming and difficult. The search space for DL hyperparameters is exponentially large, making trial-and-error evaluation challenging and time-consuming [20]. The model's performance is also influenced by the input parameters used for training. Existing research has concentrated on computing the SOC; nevertheless, it is still necessary to discover which input attributes are more important in the calculation of the SOC [21].

Hence, in this paper, the Bayesian optimisation algorithm is introduced for hyperparameter tuning of RNN algorithms (LSTM, BiLSTM and GRU), thereby overcoming the drawback of the trial and error approach. The impact of variation in the hidden neuron in the estimation accuracy is analysed for LSTM, BiLSTM and GRU. Along with the battery input parameters (current, voltage and temperature), in this

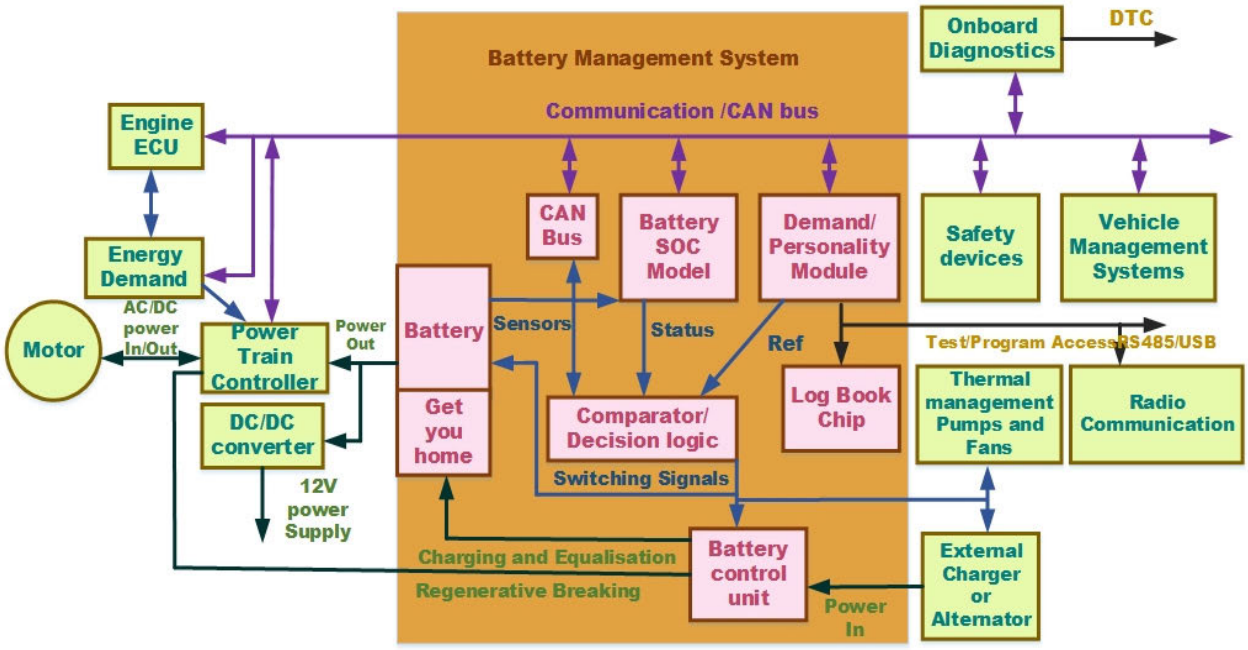

FIGURE 2. Functions of Battery Management System in Electrical Vehicle System.

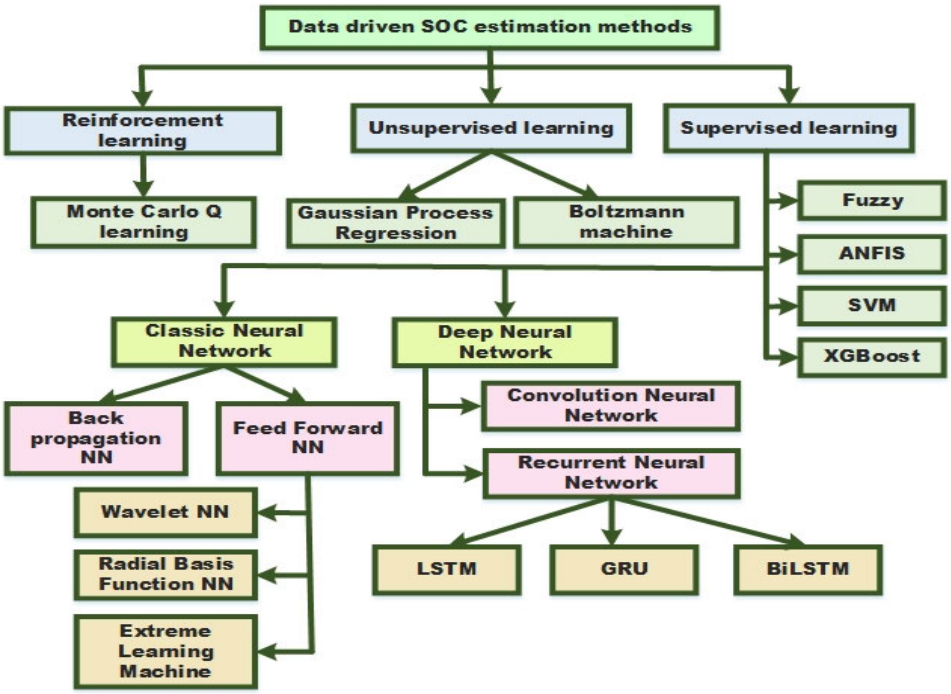

FIGURE 3. Classification of data-driven SOC estimation methods [4].

proposed work, average voltage and average current are also considered as the input parameters for SOC estimation. Since the average voltage is the average of present and past voltages, it can provide more information about the previous SOC condition. Similarly, average current can provide information regarding the present and past load connected to the battery. The significant contribution of the paper is

- Three deep learning algorithms (LSTM, GRU and BiLSM) with varied numbers of hidden neurons are examined, and their architectures and principles

TABLE 1. Parameter comparison of the proposed method with existing literature.

Ref. No	Methodology	Battery Type	Input Parameters	Output	Performance Indices
[32]	DNN	CALCE dataset	Current, voltage, Temperature	SOC	MAE, RMSE
[33]	DNN	Panasonic NCR18650PF dataset	Current, voltage, Temperature	SOC	MAE, RMSE
[34]	DNN	CALCE dataset	Current, voltage, Temperature	SOC	MAE, RMSE
[35]	LSTM	CALCE dataset	Current, voltage, Temperature	SOC	MAE, RMSE
[36]	LSTM	Panasonic NCR18650PF dataset	Current, voltage, Temperature	SOC	MAE, RMSE
[36]	BiLSTM	Panasonic NCR18650PF dataset	Current, voltage, Temperature	SOC	MAE, RMSE
[26]	GRU	Panasonic NCR18650PF dataset and CALCE dataset	Current, voltage, Temperature	SOC	MAE, RMSE
Proposed methodology	**LSTM, GRU, BiLSTM**	**Panasonic NCR18650PF dataset**	**Current, average current, temperature, voltage, average voltage**	**SOC**	**MAE, RMSE**

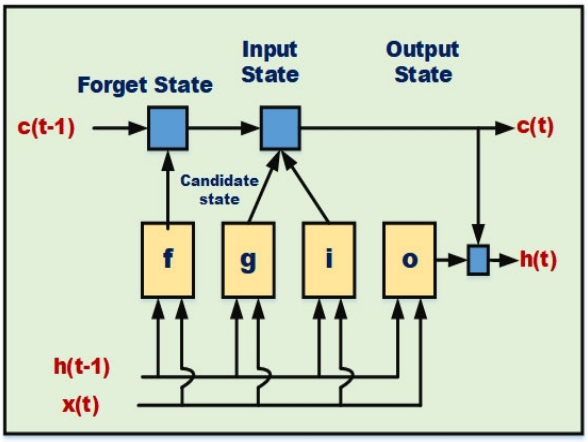

FIGURE 4. LSTM Structure [17], [36].

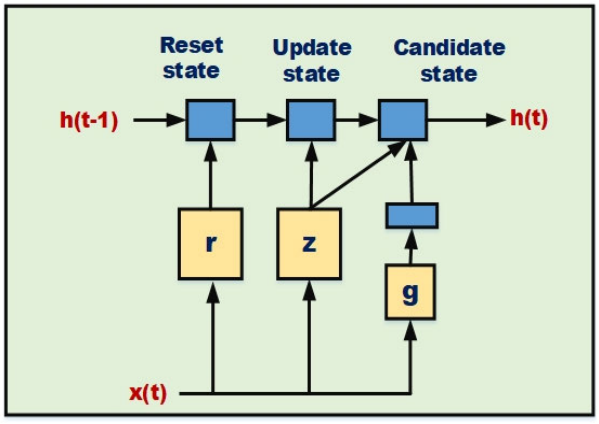

FIGURE 5. GRU Structure [19], [26].

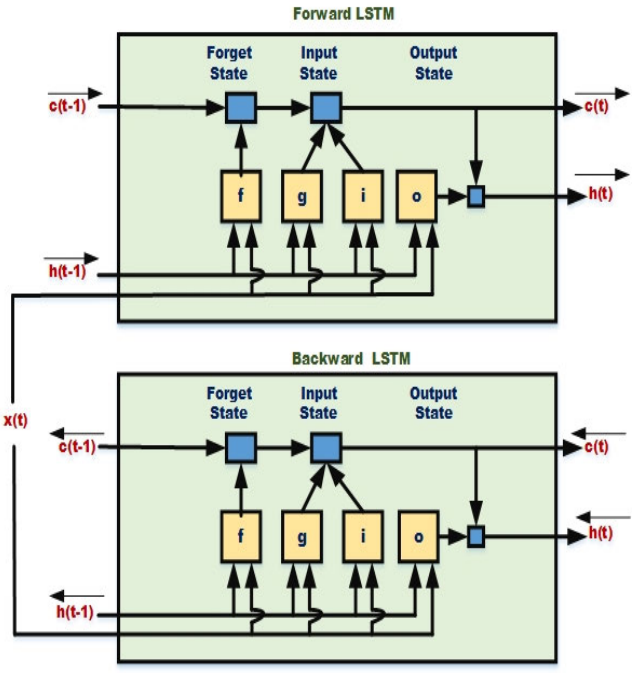

FIGURE 6. Figure BiLSTM architecture [36].

are described to elucidate their benefits for SOC estimation.

- Bayesian optimization algorithm-based hyperparameter tuning technique is proposed to compensate for the flaw of manually establishing the network parameters and helps determine the best network parameters to increase network performance.
- To verify the proposed model's accuracy at various operating temperatures (−10°C, 0°C, 10°C and 25°C), the data set obtained from Hamilton's McMaster University is used. The RMSE of the model obtained during training and testing is compared with each other and found that BiLSTM has better performance compared to LSTM and GRU for the selected input parameters (voltage, current, temperature, average temperature

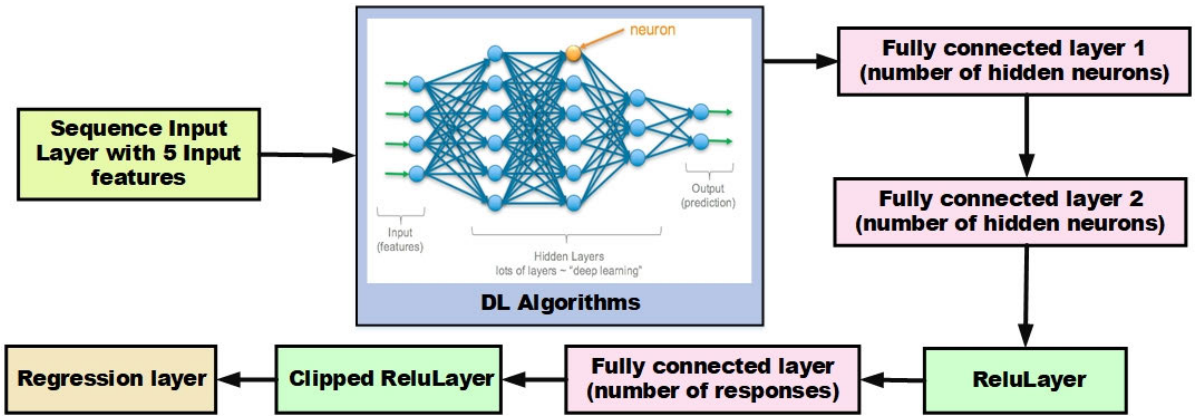

FIGURE 7. Flowchart of SOC estimation using DL algorithms.

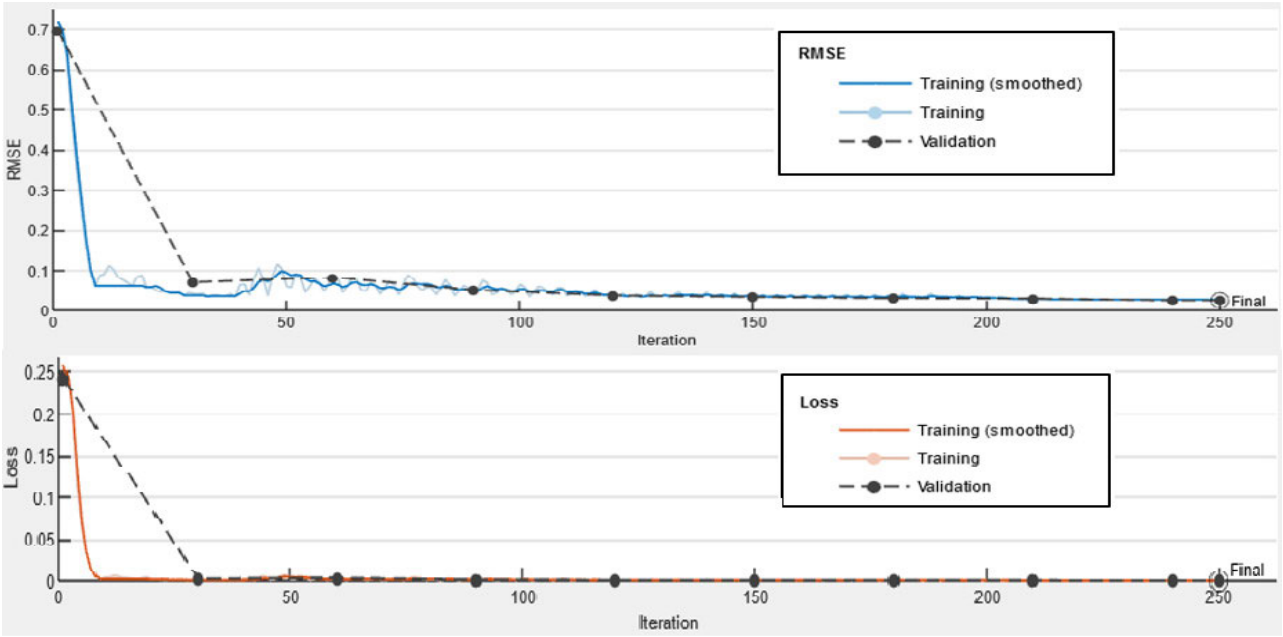

FIGURE 8. RMSE and Loss function of LSTM-based network trained with 30-neuron.

and average current) under varying numbers of hidden neurons.

II. LITERATURE REVIEW

Over the past decades, numerous SOC estimation techniques have been proposed. The coulomb counting approach and the lookup table method are the strategies that are considered to be conventional techniques. However, both methods have their limitations in serving as the better option for the SOC estimation in EVs [22], [23]. To overcome these drawbacks, numerous model-based, observer-based and filter-based approaches have been proposed. The Kalman filter is one of the filter-based techniques that has become more important for determining the battery's SOC and SOH. Despite the fact that these methods demonstrate the nonlinear features of the battery, the need for battery modelling increases the time and computing complexity [24].

In modern times, data-based SOC estimation techniques have been highly preferred by researchers for accurate SOC prediction. The recent data-driven methods applied for the SOC estimation technique are shown in Figure 3. Since SOC estimation approaches based on deep learning (LSTM, GRU, DNN, BiLSTM) can directly map sampled battery operational signals (e.g., current and voltage) to SOC and eliminate the necessity of laborious battery modelling or feature engineering, researchers are carrying out intense research in this field [14].

In [16], the LSTM with 500 hidden units is proposed for SOC estimation. The model was validated using a public dataset and obtained reduced estimation error at varying operating conditions. LSTM combined with UKF was proposed

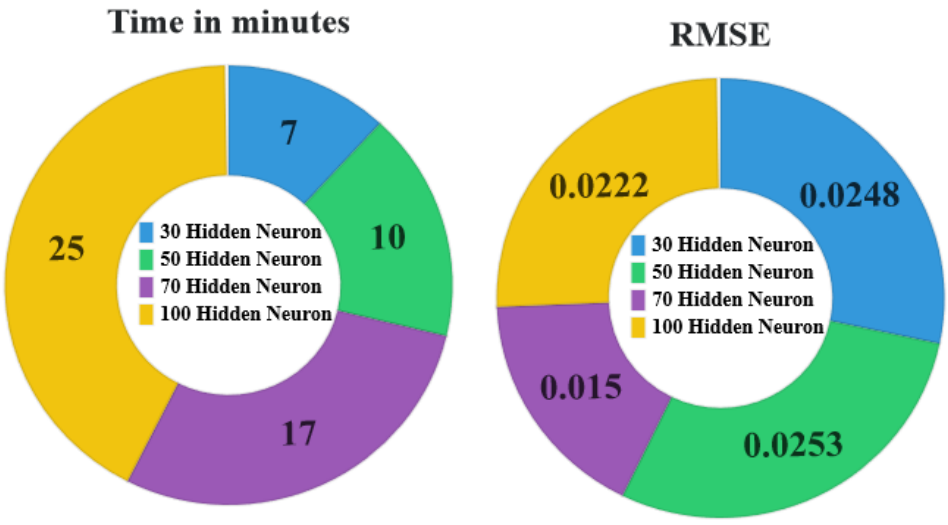

FIGURE 9. RMSE and training time of LSTM network with 30, 50, 70 and 100 hidden neuron.

in [25], which reduces the noise and improves estimation accuracy. In [26], the researcher proposed SOC estimation using GRU, which estimates with the reduced MAE of 0.86%. GRU contains 1000 hidden units connected to an FC layer with 50 nodes. The researcher validated the proposed model using two different public datasets. In this work, the researcher utilized a trial-and-error approach to find the optimal parameter.

Similarly, in [20], CNN-GRU-based SOC estimation was proposed. In this work also trial and error approach is used to find the optimal hyperparameter. BiLSTM, BiGRU, and stacked LSTM-based SOC estimation have also been proposed to estimate SOC accurately [27]. Many research articles have also been proposed that focus on the development of algorithms for optimal hyperparameter selection of RNN. The researchers have used the Ensemble algorithm [18], Particle Swarm optimisation algorithm [28], genetic algorithm [29], Momentum-based optimizer [30] and Nesterov optimizer [31] for the optimal hyperparameter selection. However, the major limitation of these methods is that the hyperparameter selection is based on selection heuristics. Hence, in the proposed work, the Bayesian optimisation technique is used for the optimal selection of hyperparameters that provide increased flexibility and a unified model capable of predicting SOC more accurately under varying ambient temperatures.

The estimation of SOC based on DL algorithms not only depends on the optimal hyperparameter selection but also the correlation of input parameters with the output SOC. From Table 1, it is observed that most of the researchers have considered only battery voltage, current and temperature as the input parameters for the estimation of SOC. Though these methods have shown encouraging results, there is still room for development as these models have only taken into account a portion of the variables that could influence predictions and have not taken environmental factors into account. In [37], the effect of auxiliary loads like heating and air conditioning should have been taken into account. Numerous studies [21] discovered that an electric vehicle's energy consumption is influenced by various factors, including traffic, road elevation, auxiliary loads, wind direction and speed, ambient temperature, and the starting battery's level of charge. The past and present voltage also act as an important factor for accurate SOC estimation. Therefore, for accurate calculation of SOC, the impact of all these elements can be considered. To fill this research gap, along with battery voltage, current and temperature, average voltage and average current are used as an input parameter for accurate SOC estimation in this study. In the future, the study will be elaborated by considering various environmental and road conditions as the input parameter for estimation.

III. OVERVIEW OF DEEP LEARNING ALGORITHM

DL algorithms are highly preferred in various disciplines of EV applications, namely in energy management, prediction of charging demand, estimation of SOH [12], vehicle detection [38], [39], [40], [41], cell balancing [5], thermal management, and so on. In this section, three types of RNN, namely LSTM, GRU and BiLSTM, applied for the estimation of SOC of EV battery is discussed.

A. LONG SHORT-TERM MEMORY

The existing RNN cannot handle lengthy input sequences due to explosion problems and the gradient vanishing problem. Therefore, an advanced gated RNN known as an LSTM is proposed to handle extended input sequences. Although the core modules or units of the LSTM and RNN networks are composed differently, they share the same topological structure. Figure 4 depicts the architecture of the LSTM network. Mapping input sequences to output sequences allows it to characterize nonlinear dynamic systems. The gating system that regulates neural information processing is added inside

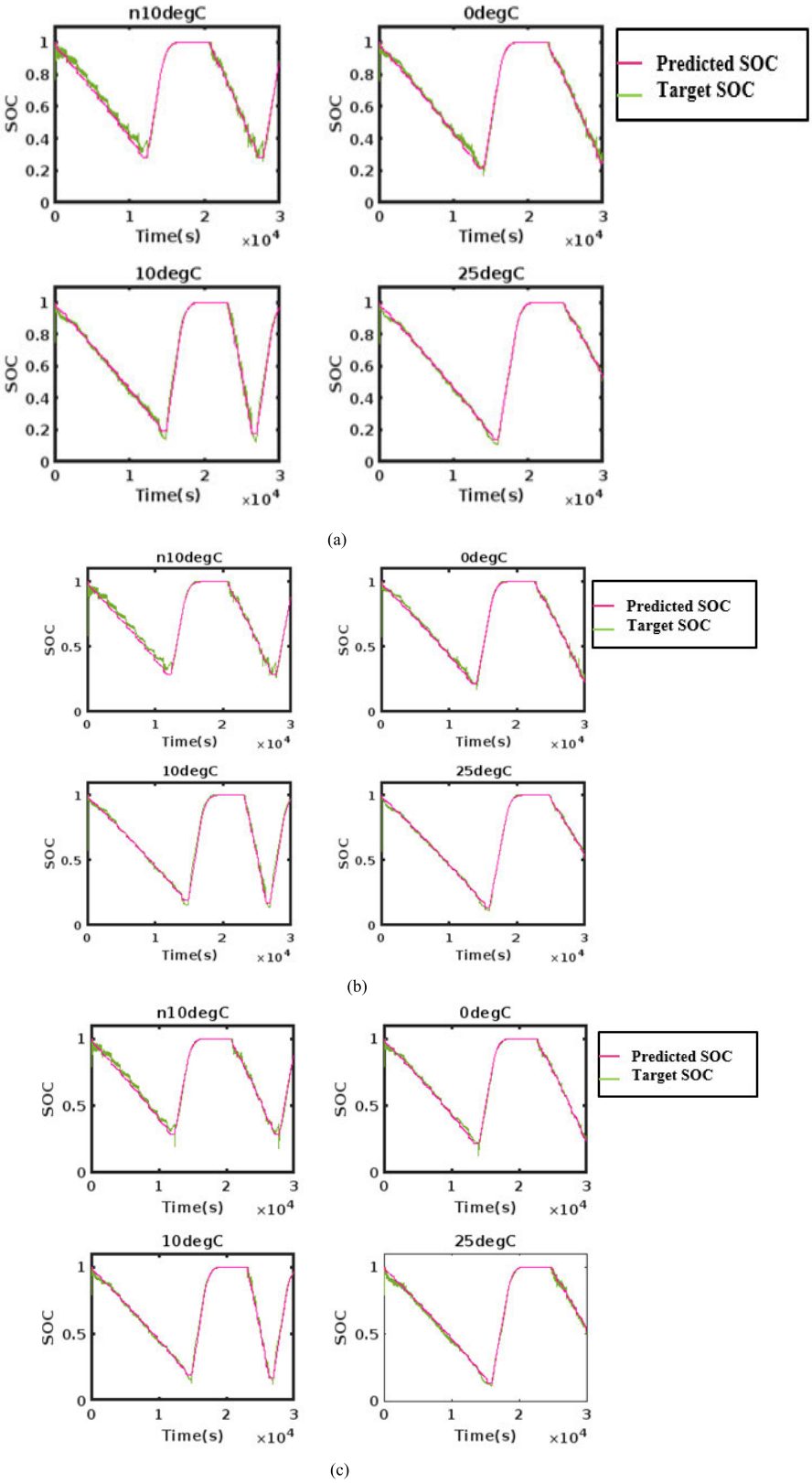

FIGURE 10. a. Predicted and targeted SOC of LSTM network with 30 hidden neurons obtained during testing. b: Predicted and target SOC of LSTM network with 50 hidden neurons obtained during testing. c: Predicted and target SOC of LSTM network with 70 hidden neurons obtained during testing.

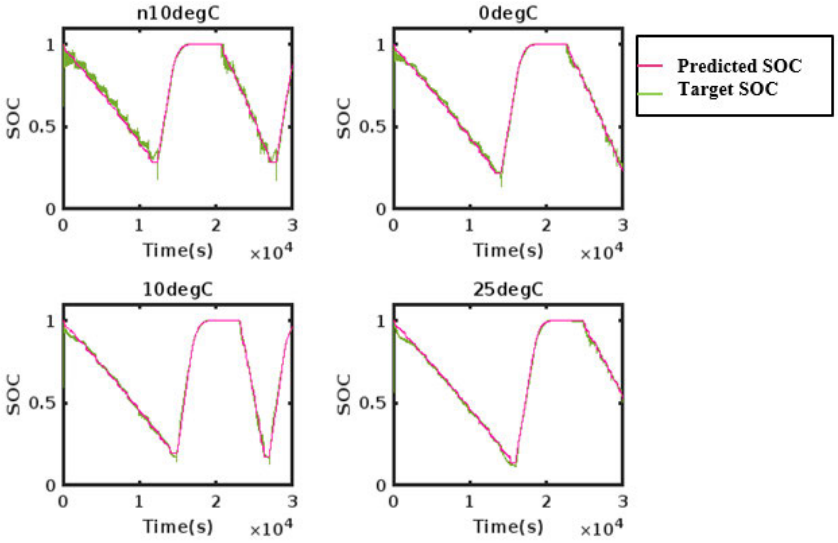

(d)

FIGURE 10. *(Continued.)* **d. Predicted and target SOC of LSTM network with 100 hidden neurons obtained during testing.**

each LSTM unit, which otherwise has the same input and output as the RNN unit. The old and new states are combined linearly to form the network's state, with some old states still existing and flowing. RNN, on the other hand, updates and replaces the state value entirely at each time step. The input, forget, and output gates are the three gates that make up an LSTM. Three gates regulate the information in the cell at time step t: the forget gate $f(t)$ manages the cell state and decides whether to remove information from the cell state. The input gate $i(t)$ updates the state value and decides whether data should be written to the cell state. The final output gate $o(t)$ generates cell state $c(t)$ and determines which data is transmitted as the hidden state output. The candidate state $g(t)$ is used to decide what information is written to the cell state. The expression for various gates of LSTM has been stated in expressions 1 to 7. The hidden state $h(t)$ is intended to encode a type of characterization of the data from the previous time step, whereas the cell state $c(t)$ is intended to encode an aggregate of the data from all previously processed time steps. The output of each cell in LSTM is generated through output state $y(t)$.σ represents the sigmoidal activation function. The model input weights (W_{xi}, W_{xf}, and W_{xo}), recurrent weights (W_{hi}, W_{hf},and W_{ho}), and biases (b_i, b_f, and b_o) are represented by the LSTM parameter matrices.

$$\text{Input gate } i(t) = \sigma\left(W_{xi}x_t + W_{hi}h_{t-1} + b_i\right) \quad (1)$$

$$\text{Forget gate } f(t) = \sigma\left(W_{xf}x_t + W_{hf}h_{t-1} + b_f\right) \quad (2)$$

$$\text{Candidate gate } g(t) = \sigma\left(W_{xg}x_t + W_{hg}h_{t-1} + b_g\right) \quad (3)$$

$$\text{Output gate } o(t) = \sigma\left(W_{xo}x_t + W_{ho}h_{t-1} + b_o\right) \quad (4)$$

$$\text{Cell state } c(t) = (f(t).c(t-1)) + (i(t).g(t)) \quad (5)$$

$$\text{Hidden state } h(t) = o(t).(\sigma c(t)) \quad (6)$$

$$\text{Output state } y(t) = \sigma(W_y(h(t)) + b_y \quad (7)$$

B. GATED RECURRENT UNIT

Li et al. proposed the Gated Recurrent Unit (GRU) in 2014 [26]. GRU can achieve long-term sequential dependence and a straightforward internal structure in all enhanced RNNs. While the LSTM-based RNN model has demonstrated the highest level of performance across various machine learning tasks, its gating mechanism has resulted in significant complexity. In contrast to the LSTM-based model, the GRU-based model requires less memory and is more effective at eliminating gradients due to its simpler structure and fewer parameters. Figure 5 depicts the GRU structure.

$z(t)$ is defined as an ''update gate'' that scales the value into *[0, 1]*. The amount of new input that should be used to update the hidden state is decided by the update gate. The ''reset gate'' is denoted by the symbol *r(t)*. It resembles the LSTM forget gate. Reset vector ''r'' specifies the extent to which the prior hidden state ought to be forgotten. Candidates' hidden state determines the historical data stored. It is usually known as the GRU cell's memory component and was estimated from the reset gate. The expression for various gates and states of GRU is given from equations 8 and 12. These include the following: $x(t)$ is the current hidden layer node's input. *h(t)* is the current hidden state, and *h(t-1)*is the output of the previously hidden layer node. GRU cell output y (t) dependents on updated hidden state $h(t)$. The model input weights (W_{xr}, W_{xz}, and W_{xg}), recurrent weights (W_{hr}, W_{hz},and W_{hg}), and biases (b_r *and* b_z) are represented by the GRU parameter matrices. σ Represents the sigmoidal activation function.

$$\text{Reset gate } r(t) = \sigma\left(W_{xr}x_t + W_{hr}h_{t-1} + b_r\right) \quad (8)$$

$$\text{Update gate } z(t) = \sigma\left(W_{xz}x_t + W_{hz}h_{t-1} + b_z\right) \quad (9)$$

$$\text{Candidate state } g(t) = \sigma\left(W_{xg}x_t + b_g\right) + \left(W_{hg}h_{t-1}.r(t)\right) \quad (10)$$

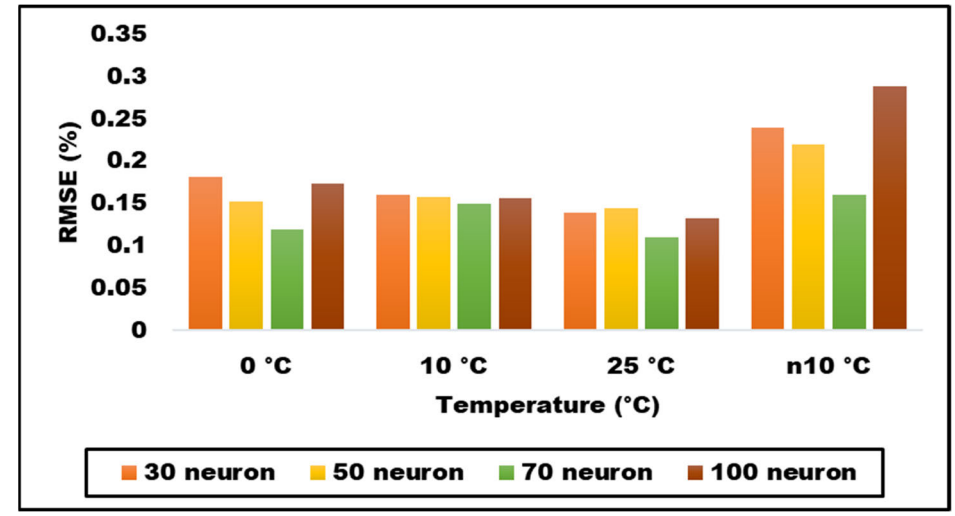

(a)

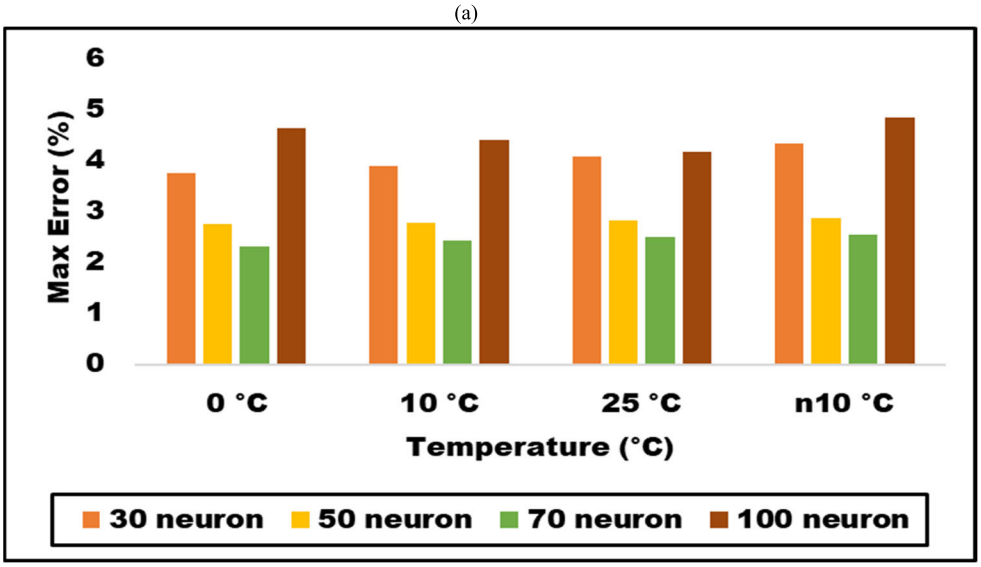

(b)

FIGURE 11. a. RMSE between predicted and target SOC of LSTM for varied hidden neuron and temperature. b. Max Error between predicted and target SOC of LSTM for varied hidden neuron and temperature.

$$\text{Hidden state } h(t) = ((1 - z(t)).g(t)) + (z(t).h(t-1)) \tag{11}$$

$$\text{Output } y(t) = \sigma(W_y(h(t)) + b_y \tag{12}$$

C. BILAYERED LSTM

The term Bidirectional LSTM, also known as BiLSTM, refers to a sequence model that has two LSTM layers: one for forward-processing input and another for backward-processing input [36]. Two unidirectional LSTMs comprise the bidirectional LSTM architecture, which processes the sequence forward and backward. The BiLSTM structure is shown in Figure 6. This architecture could see two distinct LSTM networks, one receiving the token sequence in its original order and the other inverted. The final output is the sum of the probabilities from each LSTM network, each producing a probability vector as its output. The expressions regarding forward LSTM are stated in expressions 13 to 18, for the backward LSTM from 19 to 24 and the final output gate is given in expression 25. The calculations are similar to LSTM. The hidden state output of forward LSTM $\overrightarrow{\boldsymbol{h}(t)}$ and backward LSTM $\overleftarrow{\boldsymbol{h}(t)}$ together calculates the BiLSTM cell output $\boldsymbol{y}(t)$.

Forward LSTM

$$\text{Input gate} = \sigma\left(\overrightarrow{W_{xi}}x_t + \overrightarrow{W_{hi}}\overrightarrow{h_{t-1}} + \overrightarrow{b_i}\right) \tag{13}$$

$$\text{Forget gate } \overrightarrow{f(t)} = \sigma\left(\overrightarrow{W_{xf}}x_t + \overrightarrow{W_{hf}}\overrightarrow{h_{t-1}} + \overrightarrow{b_f}\right) \tag{14}$$

$$\text{Candidate state } \overrightarrow{g(t)} = \sigma\left(\overrightarrow{W_{xg}}x_t + \overrightarrow{W_{hg}}\overrightarrow{h_{t-1}} + \overrightarrow{b_g}\right) \tag{15}$$

$$\text{Output gate } \overrightarrow{o(t)} = \sigma\left(\overrightarrow{W_{xo}}x_t + \overrightarrow{W_{ho}}\overrightarrow{h_{t-1}} + \overrightarrow{b_o}\right) \tag{16}$$

$$\text{Cell state } \overrightarrow{c(t)} = (\overrightarrow{f(t)}.\overrightarrow{c(t-1)}) + (\overrightarrow{i(t)}.\overrightarrow{g(t)}) \tag{17}$$

$$\text{Hidden state } \overrightarrow{h(t)} = \overrightarrow{o(t)}.(\sigma\overrightarrow{c(t)}) \tag{18}$$

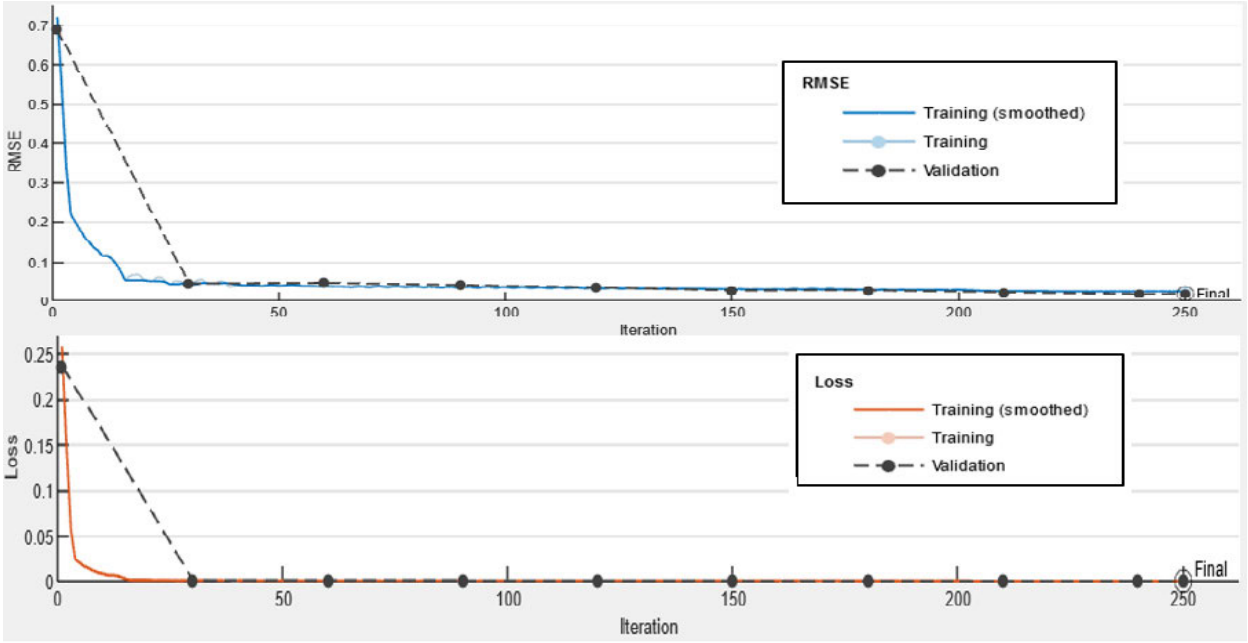

FIGURE 12. RMSE and loss function of GRU-based network trained with 30 neuron.

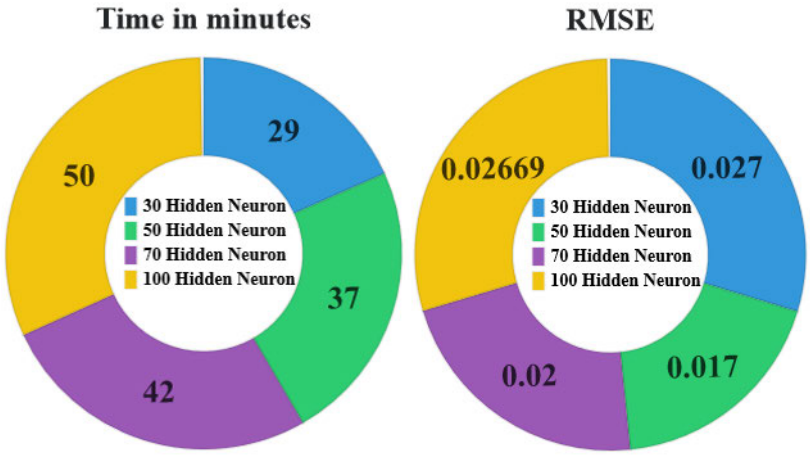

FIGURE 13. RMSE and training time of GRU network with 30, 50, 70 and 100 hidden neuron.

Backward LSTM

$$\text{Input gate } \overleftarrow{\iota(t)} = \sigma\left(\overleftarrow{W_{xl}}x_t + \overleftarrow{W_{hl}}\overleftarrow{h_{t-1}} + \overleftarrow{b_l}\right) \quad (19)$$

$$\text{Forget gate } \overleftarrow{f(t)} = \sigma\left(\overleftarrow{W_{xf}}x_t + \overleftarrow{W_{hf}}\overleftarrow{h_{t-1}} + \overleftarrow{b_f}\right) \quad (20)$$

$$\text{Candidate state } \overleftarrow{g(t)} = \sigma\left(\overleftarrow{W_{xg}}x_t + \overleftarrow{W_{hg}}\overleftarrow{h_{t-1}} + \overleftarrow{b_g}\right) \quad (21)$$

$$\text{Output gate } \overleftarrow{o(t)} = \sigma\left(\overleftarrow{W_{xo}}x_t + \overleftarrow{W_{ho}}\overleftarrow{h_{t-1}} + \overleftarrow{b_o}\right) \quad (22)$$

$$\text{Cell state } \overleftarrow{c(t)} = (\overleftarrow{f(t)} \cdot \overleftarrow{c(t-1)}) + (\overleftarrow{l(t)}.\overleftarrow{g(t)}) \quad (23)$$

$$\text{Hidden state } \overleftarrow{h(t)} = \overleftarrow{o(t)} \cdot (\sigma\overleftarrow{c(t)}) \quad (24)$$

$$\text{Output state } y(t) = \sigma\left(W_y\overrightarrow{h(t)}, \overleftarrow{h(t)}\right) + b_y \quad (25)$$

D. HYPERPARAMETERS' ROLE IN THE DL ALGORITHM

Hyperparameter tuning, sometimes referred to as hyperparameter optimisation, is the process of determining which hyperparameters are optimal to utilize. The model is optimized via the application of optimisation parameters. The most important hyperparameters of DL algorithms are learning rate, number of hidden neurons, hidden units, batch size, dropout rate, epochs, optimizer and activation function.

- Learning rate: The optimizer's step size during each training iteration is controlled by this hyperparameter. An excessively high learning rate can cause instability and divergence, whereas an excessively modest learning rate might cause sluggish convergence.

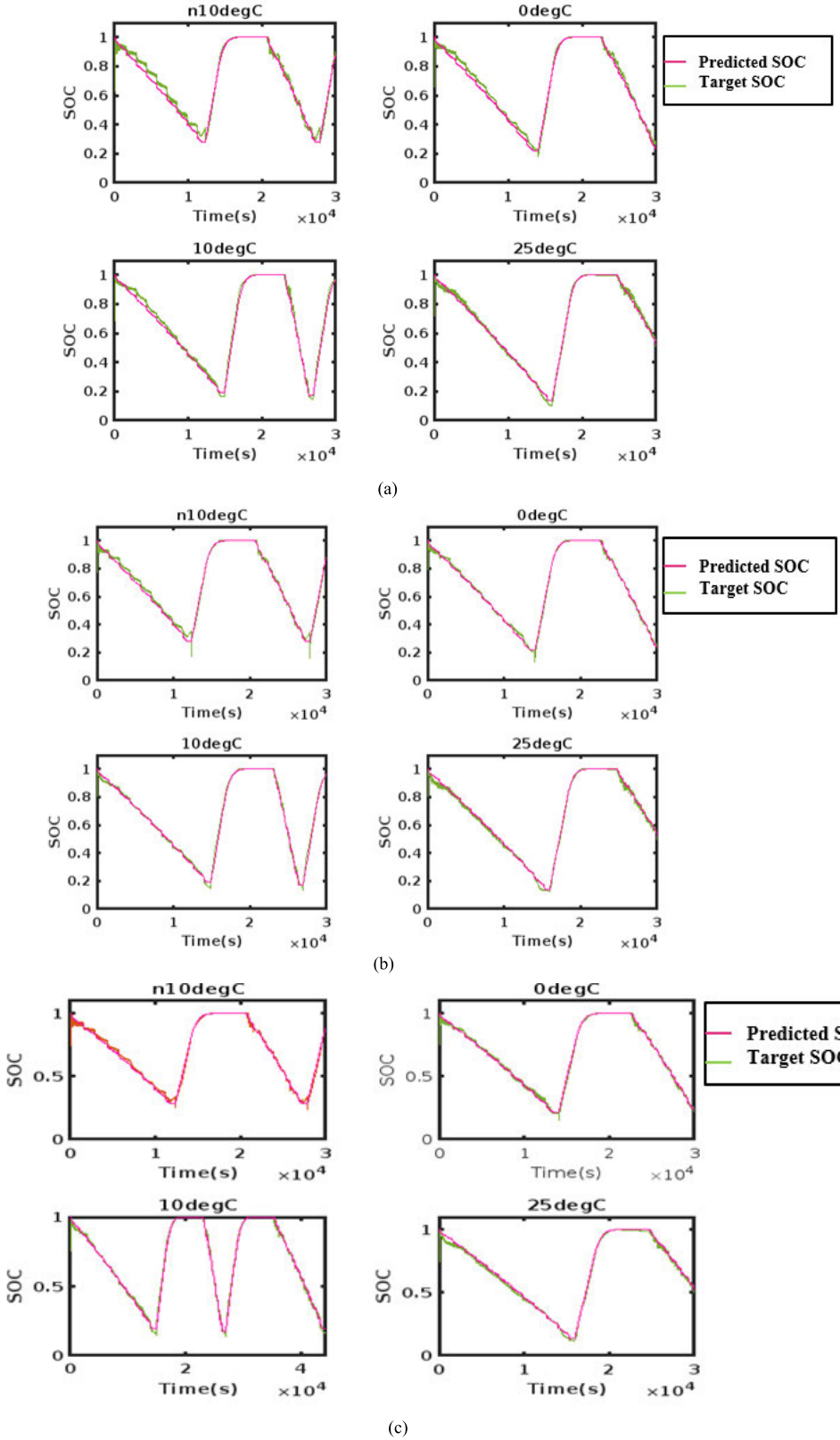

FIGURE 14. a. Predicted and target SOC of GRU network with 30 hidden neurons obtained during testing. b: Predicted and target SOC of GRU network with 50 hidden neurons obtained during testing. c: Predicted and target SOC of GRU network with 70 hidden neurons obtained during testing.

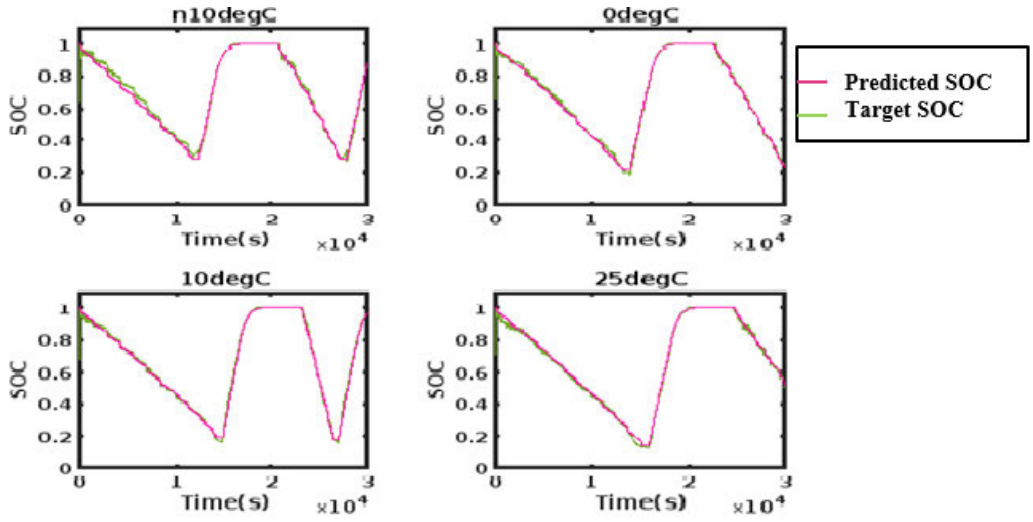

(d)

FIGURE 14. *(Continued.)* **d. Predicted and target SOC of GRU network with 100 hidden neurons obtained during testing.**

- Epochs: The number of times the model is trained using the whole training dataset is indicated by this hyperparameter. Although adding more epochs can enhance the model's performance, if done carelessly, it could result in overfitting.
- Number of layers: This hyperparameter establishes the model's depth, which can greatly affect its intricacy and capacity for learning.
- Number of layers: The hyperparameter that controls the model's width and affects its ability to depict intricate relationships in the data is the number of nodes per layer.
- Activation function: By adding nonlinearity to the model, this hyperparameter enables the model to learn intricate decision limits. Rectified Linear Unit (ReLU), sigmoid, and tanh are examples of common activation functions.
- Dropout rate: A dropout layer must be present in conjunction with each LSTM layer. This layer lessens the sensitivity to particular weights of the individual neurons by avoiding randomly chosen neurons, which helps prevent overfitting during training. Dropout layers can be applied to input layers but not output layers, as this could cause issues with the model's output and the error computation. Twenty per cent is a good place to start, but the dropout rate should be kept low (up to fifty per cent). It is commonly acknowledged that a 20% value is the optimal balance between mitigating the risk of overfitting and maintaining model accuracy.

IV. DATASET PREPARATION AND SELECTION OF HYPERPARAMETER

The data for training and testing is obtained from Hamilton's McMaster University. In an eight cubic foot thermal chamber, a brand-new 3Ah LG HG2 cell was tested using a 75 amp, 5-volt Digatron Firing Circuits Universal Battery Tester channel, which provided voltage and current accuracy within 0.1% of full scale. The training data is a single sequence of experimental data taken during a driving cycle in which the battery-powered electric vehicle was at 25 degrees Celsius. Around 6 lakh data is used for testing, and 39000 for validation. Four experimental data sequences, at four distinct temperatures, −10°C, 0°C, ten °C and 25°C, consisting of around 30000 data in each set, obtained during driving cycles are included in the test data.

The selection of hyperparameters, namely the number of hidden neurons, hidden layers, learning rate, activation function and so on, plays a major role in the performance of RNN. An increase in hyperparameters leads to an exponential increase in the search space. In addition, each hyperparameter influences the other, and hence, the negotiation of these parameters may lead to suboptimal solutions. Conventionally, grid search and random search are the methods used for hyperparameter tuning. However, due to their vast space usage, high time consumption to train a single model and computationally expensive nature, they are not highly preferred. Hence probabilistic model, namely Bayesian Optimization (BO), is preferred for hyperparameter tuning.

In contrast to GS and RS, BO bases its determination of future evaluation points on the outcomes of past assessments. A surrogate model and an acquisition function are two essential elements that BO employs to identify the subsequent hyper-parameter configuration. All currently observed points are to be fitted into the objective function by the surrogate model. The acquisition function balances the trade-off between exploration and exploitation to select the usage of various points after getting the prediction distribution of the probabilistic surrogate model. The variants of the Bayesian optimizer are the tree-structured Parzen estimator and the Gaussian Process estimator. In the proposed work BO-GP

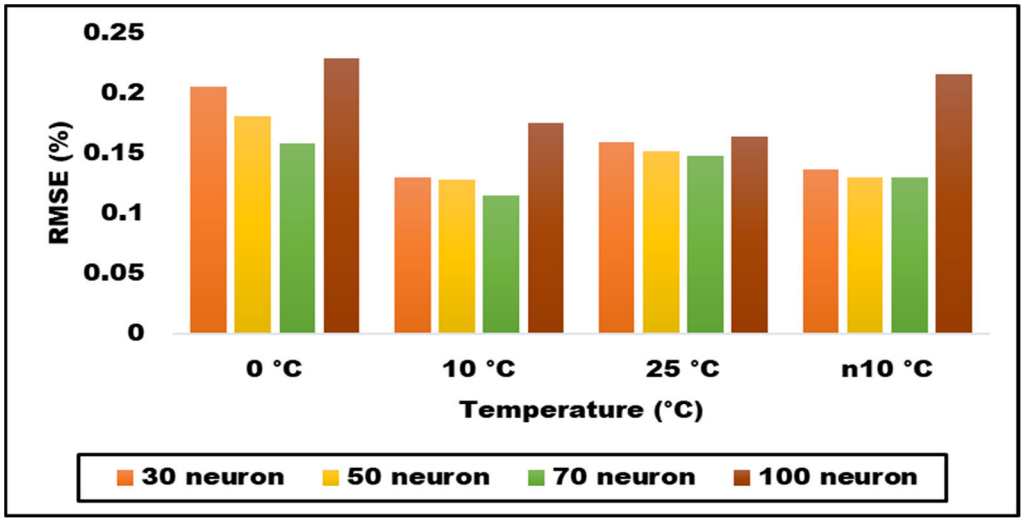

(a)

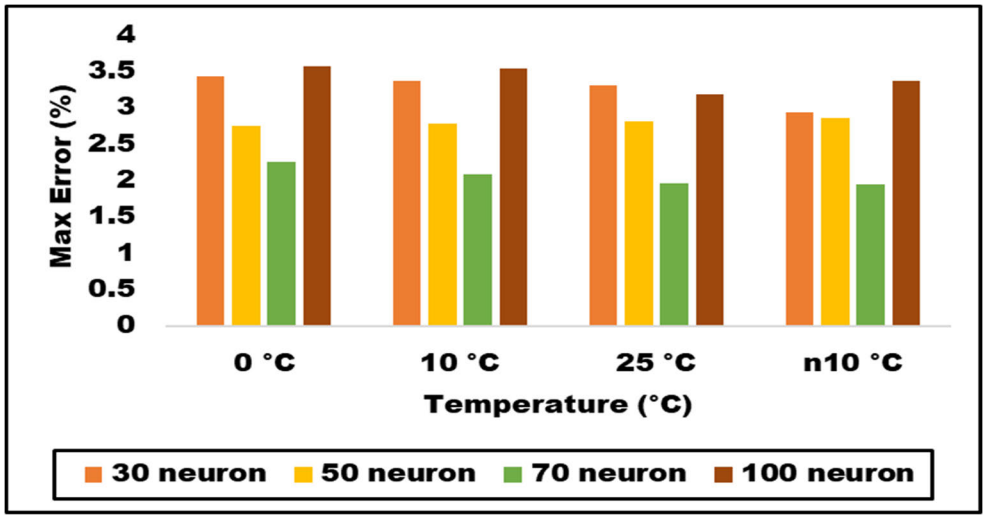

(b)

FIGURE 15. a. RMSE between predicted and target SOC of GRU for varied hidden neuron and temperature. b: Max Error between predicted and target SOC of GRU for varied hidden neuron and temperature.

is used due to their ability to reduce the mean square error during estimation.

Twenty random searches and ten iterations of Bayesian optimization are used in this instance. Upon optimization, 0.001 and 0.2 are the determined learning and dropout rates. The effect of variation in the number of hidden neurons in the DL algorithm is considered for analysis in this work. The various other parameter set during the algorithm's execution is listed in Table 2.

TABLE 2. Training parameters of DL algorithms.

S.No.	Training Parameter	Value
1	optimizer	Adam
2	Epoch	250
3	iteration	250
4	Validation frequency	30 iteration
5	Hardware resource	Single CPU
6	Learning rate schedule	Piecewise
7	Learning rate	0.001
8	Dropout rate	0.2

V. EXPERIMENTAL RESULT AND DISCUSSION

From the theoretical analysis, it is found that RNN algorithms (LSTM, GRU and BiLSTM) can be best suitable for performing SOC estimation compared to other SOC estimation algorithms. The experiment is conducted in Matlab Software installed in a single PC system. The proposed architecture includes a single Sequence input layer, an RNN layer, two fully connected layers, and a clippedRelu layer followed by a regression layer. In this research, various parameter settings for SOC estimation are constructed, and the effects of varying

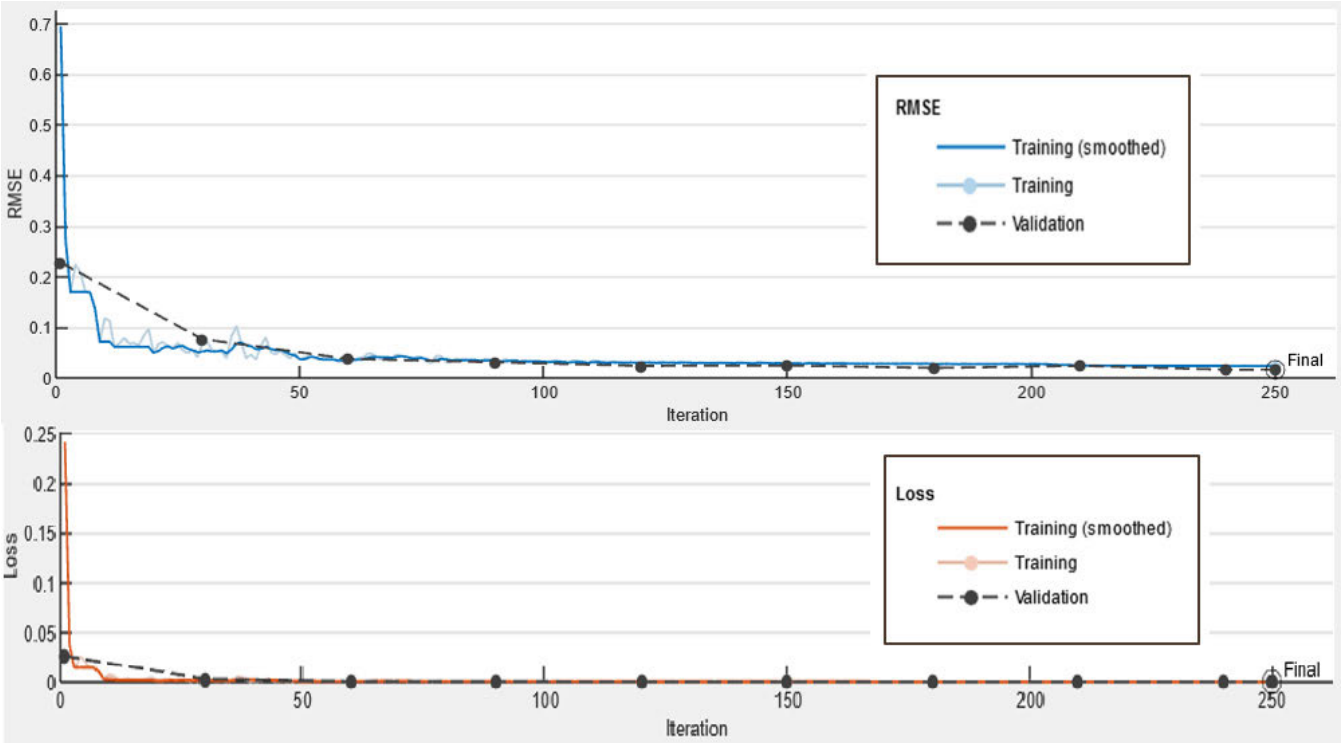

FIGURE 16. RMSE and Loss function of BiLSTM network trained with 30-neuron.

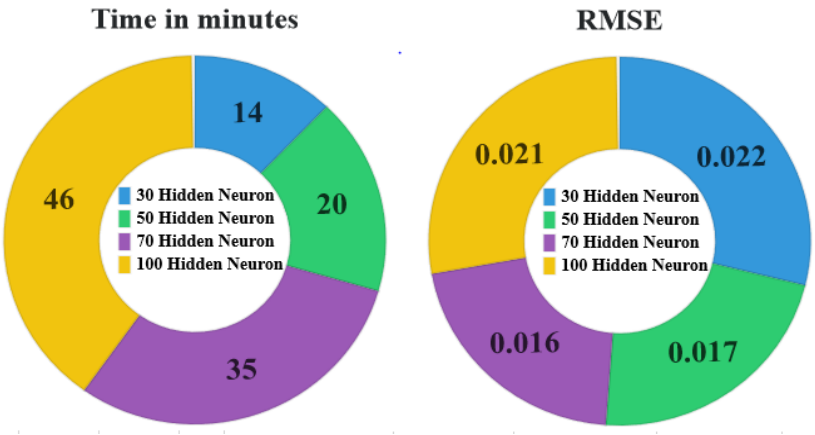

FIGURE 17. RMSE and training time of BiLSTM network with 30, 50, 70 and 100 hidden neuron.

hidden layer neuron numbers on the model are specifically discussed to investigate the effects of these settings on the model estimation performance.

Following the establishment of the structure, the network has to be trained. Prior to training, the input data set is normalized using min-max normalization function to scale the input values between 0 and 1. This process is followed by the implementation of Bayesian optimisation network. To optimize the DL networks during training process, the Adam optimization algorithm is used. In the proposed work, the number of input features is 5, and the output response is 1. The Tanh function is used as the state activation function, and the sigmoid function is used as the gate activation function. To prevent the exploding of the gradient, the value of the gradient threshold is set to be one and to avoid the padding of sequence; the minimum batch size is maintained to be 1. Mean Square Error is selected as the loss function. The general architecture of the proposed DL algorithms for SOC estimation using LSTM is shown in Figure 7.

A. LSTM-BASED SOC ESTIMATION

The performance of the proposed LSTM network for estimating SOC is analyzed through performance matrices, namely RMSE and loss function (MSE). Initially, the proposed network is trained with 30 hidden neurons. The obtained training

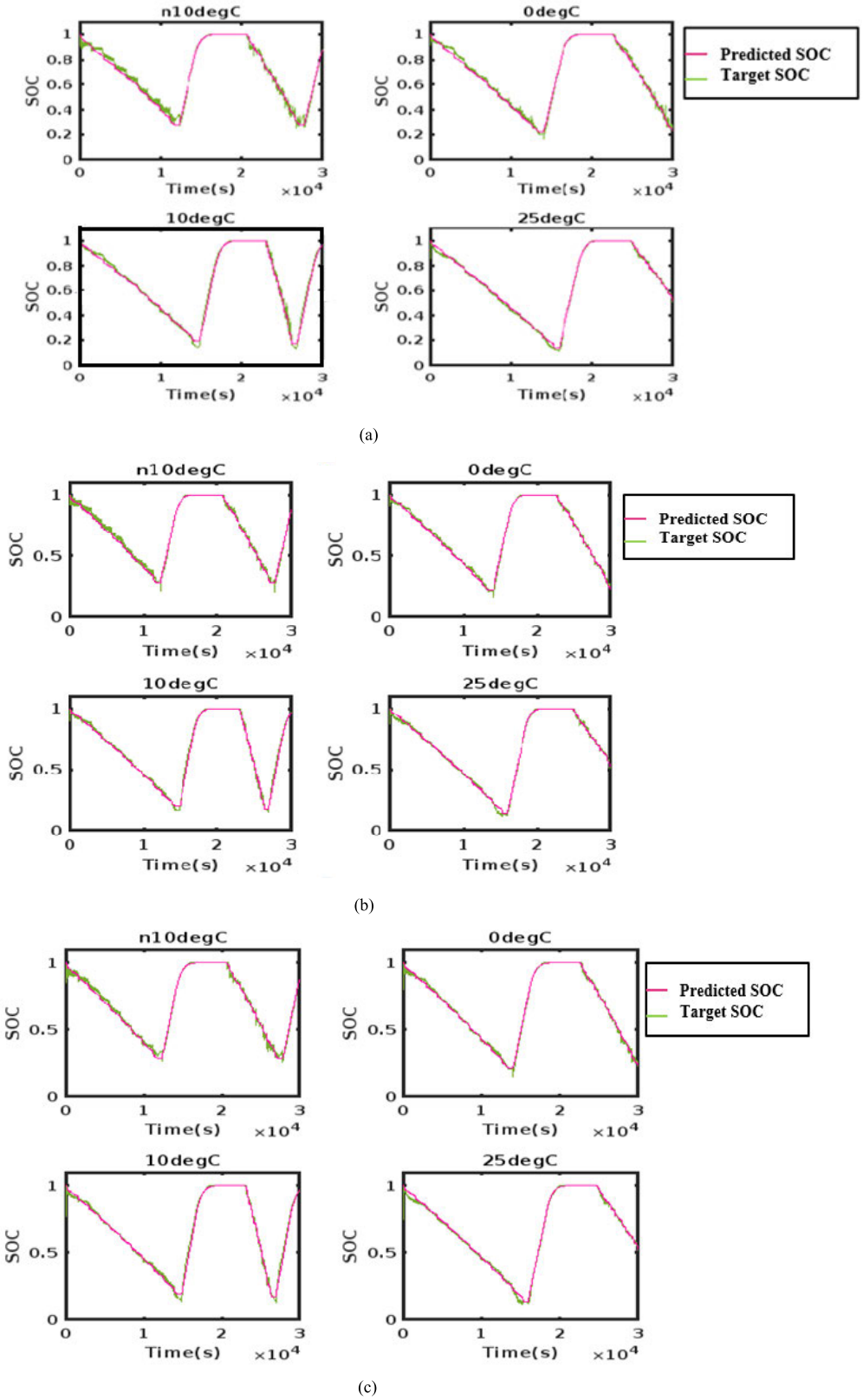

FIGURE 18. a. Predicted and target SOC of BiLSTM network with 30 hidden neurons obtained during testing. b. Predicted and target SOC of BiLSTM network with 50 hidden neurons obtained during testing. c. Predicted and target SOC of BiLSTM network with 70 hidden neurons obtained during testing.

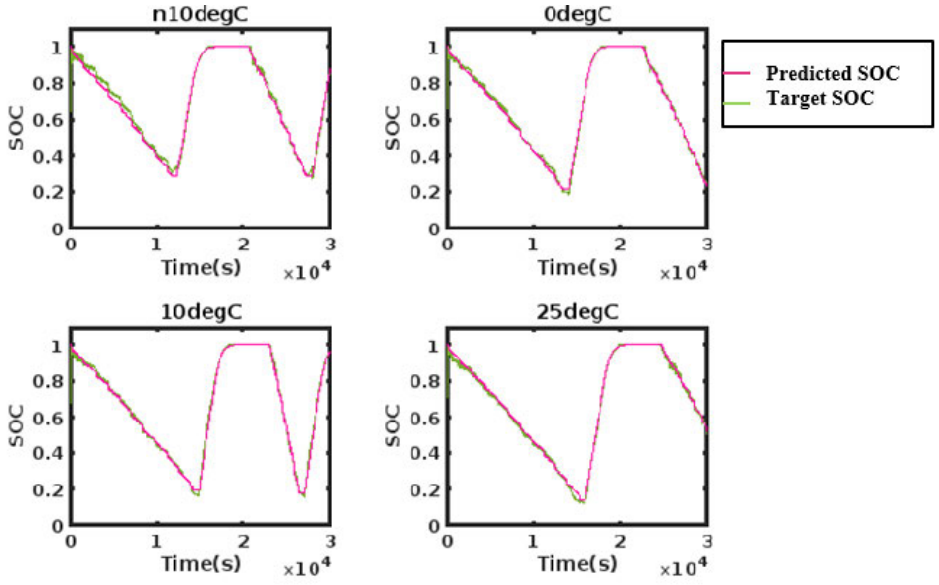

(d)

FIGURE 18. *(Continued.)* **d. Predicted and target SOC of BiLSTM network with 100 hidden neurons obtained during testing.**

results are plotted in figure 8. The obtained RMSE during training is 0.024, and the training time is 7 minutes. The number of hidden neurons is varied and analyzed to analyse the proposed network's performance in varied hyperparameter tuning environments. The number of hidden neurons varies from 30, 50, 70 and 100.

The RMSE value of obtained networks and their corresponding training time are shown in Figure 9. The figure shows that the number of hidden layer neurons increases, and estimation accuracy increases. Compared to the other models, estimation accuracy is maximum when the number of hidden layer neurons is 70; it begins to decline when the number of hidden layer neurons reaches 100. To prove the generalization of the network, the trained networks are tested with four different data sets obtained at varied temperatures (−10 °C, 0 °C, 10 °C and 25 °C) consisting of nearly 30000 data in each set.

The estimated outcomes of the model, based on the quantity of various hidden neurons at (−10 °C, 0 °C, 10 °C, and 25 °C, respectively), are shown in figures 10a to 10d. Figures 11a and 11b show the associated errors. Furthermore, the figure shows that, at room temperature, the curve representing the estimation results is relatively smooth; however, the degree of fitting with the actual measurement curve is relatively poor, resulting in low estimation accuracy at higher or lower temperatures, particularly near the end of the discharge, the curve representing the model estimation result is relatively steep, but the overall degree of fitting with the actual measurement curve is appropriate.

B. GRU-BASED SOC ESTIMATION

GRU-RNN network model comprises a sequence input layer, a GRU network layer, a fully connected layer with neurons, a clippedRelu layer and a regression output layer, as illustrated in Figure 7. The battery SOC at the moment is the output of the GRU network model, which takes current, voltage, average current, average voltage and temperature measurement signals as inputs. The nonlinear relationship between inputs and SOC was found in the training set. The leaky ReLU layer provided an execution threshold. Any input value less than zero was primarily multiplied by a fixed factor coefficient.

Like LSTM, Different GRU models with varying numbers of hidden neurons (30, 50, 70, and 100) are built in this proposed work. There is a maximum epoch of 250 and a validation frequency of 30. The RMSE and loss function acquired during the GRU model's 30-hidden neuron training are shown in Figures 12 respectively.

Figures 13 display the RMSE value of the developed networks along with the corresponding training time. It is evident from the figure that as the quantity of hidden layer neurons rises, so does the estimation accuracy. When there are 50 hidden layer neurons, estimation accuracy is at its highest compared to the other models; it starts to decrease when there are 100 hidden layer neurons. The more hidden units there are, the longer it takes to analyze the data.

Figures 14a to 14d show the discrepancy between the trained network's predicted and targeted SOC after testing it using four distinct data sets. Plots of the RMSE and MAE for test data at four distinct temperatures are shown in Figures 15a and 15b. The figure indicates that at lower RMSE and MAE values, there is a higher chance of an accurate SOC prediction. Furthermore, the figure shows that, at room temperature, the curve representing the estimation results is relatively smooth; however, the degree of fitting with the actual measurement curve is relatively poor, resulting in low estimation accuracy at higher or lower temperatures.

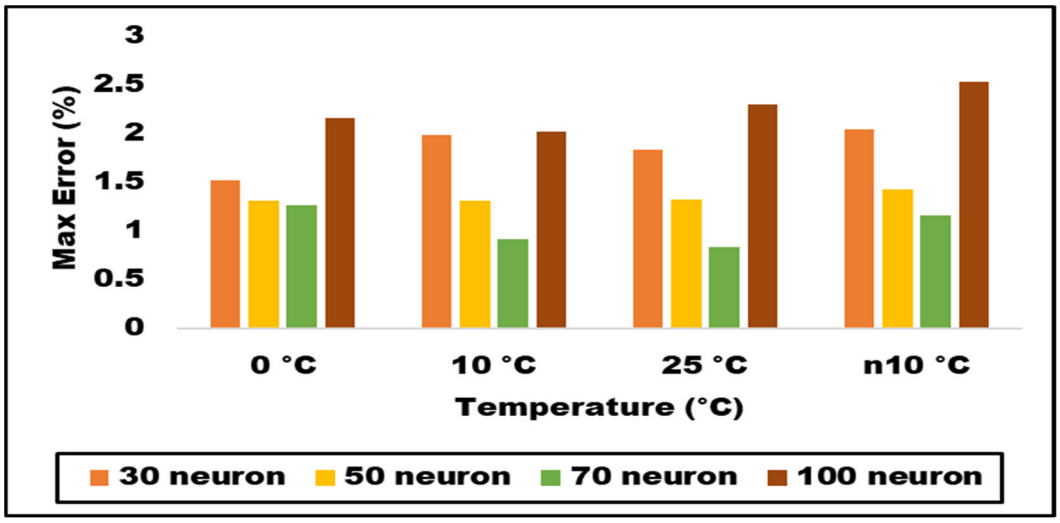

(a)

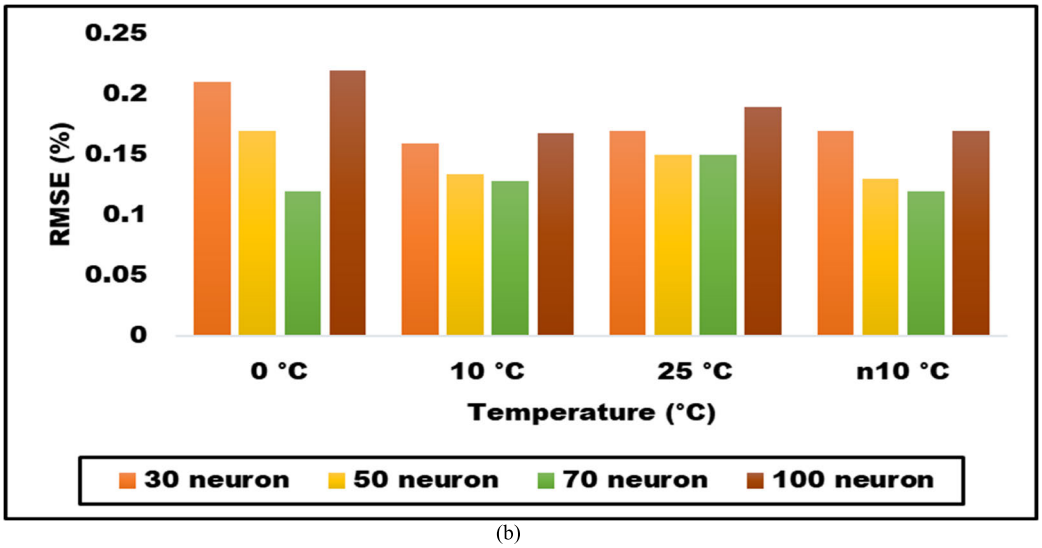

(b)

FIGURE 19. a. RMSE between predicted and target SOC of BiLSTM for varied hidden neuron and temperature. b. Max Error between predicted and target SOC of BiLSTM for varied hidden neuron and temperature.

C. BILSTM-BASED SOC ESTIMATION

SOC estimation using bidirectional long short-term memory (Bi-LSTM) has been performed. The forward and backward temporal dependencies of battery sequential data can be captured by the bidirectional LSTM, in contrast to the standard unidirectional LSTM. The state is not shared by two LSTMs moving in opposite directions. The forward LSTM's output state is exclusively transmitted to the forward LSTM, while the backward LSTM's output state is exclusively transmitted to the backward LSTM. It is not possible to connect the forward and backward LSTMs directly. At every time step, the input sequence is passed to the forward and backward LSTM layers, respectively, and the corresponding states are used to generate the outputs. The two outputs are then combined and integrated into the final output by connecting to the output layer.

STM before training the model are:

- Data normalization: preprocessing Data to avid the scale that influences the indicators. In the proposed work, data normalization is carried out through the zero-centre normalization technique.
- Building the model: As with LSTM, BiLSTM also includes a sequence input layer, clipped Relu layer, fully connected layer BiLSTM layer and regression layer.
- Selection of Optimizer: Adam optimizer is selected to prevent the gradient from explosion.
- The Selection of hyperparameters includes the number of hidden layers, hidden neurons, hidden units, epochs, batch size, iteration count, validation frequency and Dropout rate.

In BiLSTM, the width of the layer is determined by the number of neurons that are present in the hidden layer. The

TABLE 3. Overall performance comparison of the proposed algorithm during training and testing.

Algorithm	Number of hidden layers	Number of hidden neurons	Training RMSE at validation frequency 30	Testing							
				0 °C		10 °C		25 °C		-10°C	
				RMSE (%)	Max ERROR (%)	RMSE (%)	Max ERROR (%)	RMSE (%)	Max ERROR (%)	RMSE (%)	Max ERROR (%)
LSTM	2	30	0.0248	0.24	2.3236	0.16	2.4202	0.182	2.4905	0.139	2.5509
	2	50	0.025318	0.12	2.75998	0.15	2.784	0.11	2.815	0.16	2.874
	2	**70**	**0.015**	**0.222**	**3.74352**	**0.158**	**3.9012**	**0.153**	**4.0663**	**0.1445**	**4.324**
	2	100	0.0222	0.133	4.836	0.2889	4.182	0.156	4.396	0.1732	4.632
GRU	2	30	0.027	0.2297	3.43246	0.1757	3.538	0.164	3.3086	0.1304	3.3677
	2	50	0.017	0.159	2.7599	0.115	2.78	0.164	2.81	0.216	2.87
	2	**70**	**0.020**	**0.1809**	**2.2568**	**0.1288**	**1.9587**	**0.152**	**2.089**	**0.1370**	**1.9425**
	2	100	0.02669	0.206	3.567	0.13	3.3777	0.148	3.182	0.13	2.917
BiLSTM	2	30	0.022	0.220	1.262	0.1677	1.307	0.190	1.326	0.120	1.429
	2	50	0.017	0.1702	1.519	0.1288	1.982	0.170	2.3033	0.1702	2.526
	2	**70**	**0.016**	**0.12**	**1.327**	**0.16**	**0.822**	**0.15**	**0.933**	**0.12**	**1.156**
	2	100	0.021	0.2105	2.155	0.134	2.019	0.150	1.834	0.167	2.039

TABLE 4. Performance comparison of the proposed method with the existing literature.

Ref No.	Algorithm	Input and output	Hyperparameter Tuning	Performance metric
[32]	DNN	Inputs = (V, I, T) Output=(SOC)	Number of hidden layers = 2 Hidden neurons per hidden layer = 5	RMSE = 1.4% (FUDS) at 25°C RMSE = 1.5% (US06) at 25°C
[33]	DNN	Inputs = (V, I, T) Output=(SOC)	Number of hidden layers = 4 Hidden neurons per hidden layer = 50	RMSE = 0.78% (US06) at 25°C MAE = 0.61% (US06) at 25°C
[34]	DNN	Inputs = (V, I, T) Output=(SOC)	Number of hidden layers = 4 Hidden neurons per hidden layer = 64	RMSE = 3.68% at 25°C(DST, FDUS, US06, and BJDST)
[35]	LSTM	Inputs = (V, I, T) Output=(SOC)	Number of LSTM neurons = 256	RMSE = 1.71% (UDDS) at 25°C MAE = 1.39% (UDDS) at 25°C
[36]	LSTM	Inputs = (V, I, T) Output=(SOC)	Number of LSTM neurons = 32	RMSE = 0.9% (FUDS) at 25°C MaxE = 2.7% (FUDS) at 25°C
[36]	BiLSTM	Inputs = (V, I, T) Output=(SOC)	Hidden neurons = 64 Numbers of BLSTM layers = 2	MAE = 0.84% (FUDS) at 25°C MaxE = 3.46% (FUDS) at 25°C
[26]	GRU	Inputs = (V, I, T) Output=(SOC)	Number of Hidden neurons = 1000	MAE = 0.86% (FUDS) at 25°C - MaxE = 3.13% (FUDS) at 25°C
Proposed methodology	Bayesian optimized BiLSTM	Inputs = (V, I, T, average V and average I) Output=(SOC)	Number of hidden neuron=70	At 0 °C, RMSE=**0.12**% & MaxE = **1.327**% At 10 °C, RMSE=**0.16**% & MaxE = **0.822**% At 25°C, RMSE=**0.15** % & MaxE = **0.933**% At -10 °C, RMSE=**0.12**% & MaxE = **1.156**%

work that is being proposed comprises the construction of various BiLSTM models, each of which is comprised of two hidden layers that contain a different number of hidden neurons (30, 50, 70, and 100). With a validation frequency of thirty, the maximum epoch that can be used is set to be 250. The root mean square error (RMSE) and loss function found during the training of the BiLSTM model with thirty hidden neurons are depicted in Figure 16. Figure 17 illustrates the amount of time that the models need to complete their training, as well as the related root mean square error (RMSE) for various hidden neurons. The picture makes it abundantly clear that the estimation accuracy improves in proportion to the number of neurons in the hidden layer. As compared to the other models, the estimation accuracy reaches its highest

point at fifty and seventy neurons in the hidden layer, and it starts to decrease at one hundred neurons in the hidden layer.

The difference between the anticipated and targeted SOC is given in Figures 18a to 18d. This evaluation was performed on the trained network using four distinct data sets. The RMSE and MAE charts for the test data are displayed in Figures 19a and 19b. These plots are displayed at four different temperatures. The image illustrates that the probability of making an accurate prediction of the SOC increases as the RMSE and MAE values decrease. In addition, the picture illustrates that the curve that corresponds to the estimation findings is generally smooth when the temperature is at room temperature. However, when the temperature is lower, the degree of fitting with the actual measurement curve is rather bad, which results in a low estimation accuracy.

The overall performance comparison of the proposed Bayesian-optimized deep learning methods is shown in Table 3. From the table, the significant observations can be concluded that

1. The estimation accuracy is high at the room temperature but gets reduced when the temperature becomes very low. This is due to the nonlinear characteristics of the battery.
2. The number of neurons should be manageable, as they lead to overfitting and underfitting problems. Hence, 70 hidden neuron counts give the best performance in the proposed work compared to 30 and 100 neurons.

Table 4 presents the results of a comparison between the suggested method and the one that is currently in use. Upon examination of the table, it is evident that the deep learning algorithms that have been suggested and optimized using the Bayesian algorithm have a greater level of accuracy. When compared to Bayesian-optimized LSTM and GRU, the performance of BiLSTM in comparison is superior.

VI. CONCLUSION

This paper proposes a Bayesian-optimized deep learning method for SOC estimation. From the experimental results, it is found that the performance of DL algorithms increases with the selection of optimal hyperparameters. The proposed work offers several contributions. Initially, the proposed approach can estimate the SOC of the battery without having prior knowledge of the battery model and the requirement of filters and observers.

Secondly, the employment of a Bayesian optimisation algorithm for the selection of optimal hyperparameters reduces the estimation error and increases the system efficiency.

Finally, the performance of the proposed work is analysed for varying numbers of hidden neurons. The data set for analysis was obtained from Hamilton's McMaster University and maps the relationship of input parameters (current, voltage, temperature, average voltage, average current and temperature) to the output SOC. The experimental analysis is carried out in MATLAB software. The suggested techniques undergo validation and testing on four distinct datasets at four distinct temperature ranges: −10°C, 0°C, 10°C, and 25°C. The results show that the optimal design produces SOC estimations with less than 2% root mean square and 5% maximum error for all three types of RNNs (LSTM, GRU and BiLSTM). Out of the three, BiLSTM estimates SOC with less estimation error than the other two approaches since each fully connected layer has seventy hidden neurons. (RMSE = 0.12% & MaxE = 1.327% at 0 °C; RMSE = 0.16% at 10 °C; MaxE = 0.822% at 25 °C; RMSE = 0.15% at 25 °C; MaxE = 0.933% at −10 °C; RMSE = 0.12% & MaxE = 1.156%). The experimental results show that the estimation accuracy is high at room temperature but gets reduced when the temperature becomes very low. This is due to the nonlinear characteristics of the battery. Estimation of SOC with varied hidden neurons is analyzed, and it was found that the number of the neurons should neither be too small nor too high as they lead to overfitting problems. Hence, 70 hidden neuron counts give the best performance in the proposed work compared to 30 and 100 neurons.

In future work, numerous input parameters for the accurate estimation of SOC by considering environmental conditions, wind speed, vehicle velocity, and road conditions and applying attention mechanisms to select the input parameters that provide more information regarding output SOC will be done. The selected input parameters will be validated using DL algorithms, and their performance will be compared to the estimation made by graph convolutional networks.

ACKNOWLEDGMENT

The authors would like to acknowledge the support from the School of Electrical Engineering, Vellore Institute of Technology, Vellore, India. They would also like to thank the Management of Vellore Institute of Technology, Vellore for the facilities provided during the execution of this work.

REFERENCES

[1] M. Lennan and E. Morgera, "The Glasgow climate conference (COP26)," *Int. J. Mar. Coastal Law*, vol. 37, no. 1, pp. 137–151, 2022.
[2] Y. Khawaja, N. Shankar, I. Qiqieh, J. Alzubi, O. Alzubi, M. K. Nallakaruppan, and S. Padmanaban, "Battery management solutions for Li-ion batteries based on artificial intelligence," *Ain Shams Eng. J.*, vol. 14, no. 12, 2023, Art. no. 102213.
[3] R. Irle, "EV-volumes-The electric vehicle world sales database," *Glob. EV Sales*, 2021.
[4] F. Nadeem, S. M. S. Hussain, P. K. Tiwari, A. K. Goswami, and T. S. Ustun, "Comparative review of energy storage systems, their roles, and impacts on future power systems," *IEEE Access*, vol. 7, pp. 4555–4585, 2019.
[5] V. Selvaraj and I. Vairavasundaram, "Flyback converter employed non-dissipative cell equalization in electric vehicle lithium-ion batteries," *e-Prime-Adv. Elect. Eng., Electron. Energy*, vol. 5, Sep. 2023, Art. no. 100278.
[6] P. U. Nzereogu, A. D. Omah, F. I. Ezema, E. I. Iwuoha, and A. C. Nwanya, "Anode materials for lithium-ion batteries: A review," *Appl. Surf. Sci. Adv.*, vol. 9, Jun. 2022, Art. no. 100233.
[7] L. Wang, X. Zhao, Z. Deng, and L. Yang, "Application of electrochemical impedance spectroscopy in battery management system: State of charge estimation for aging batteries," *J. Energy Storage*, vol. 57, Jan. 2023, Art. no. 106275.
[8] J. P. Christophersen, "Battery test manual for electric vehicles, revision 3," Idaho Nat. Lab., Idaho Falls, ID, USA, Tech. Rep. INL/EXT-15-34184, 2015.
[9] M. J. Lain and E. Kendrick, "Understanding the limitations of lithium ion batteries at high rates," *J. Power Sour.*, vol. 493, May 2021, Art. no. 229690.

[10] J. Liu and X. Liu, "An improved method of state of health prediction for lithium batteries considering different temperature," *J. Energy Storage*, vol. 63, Jul. 2023, Art. no. 107028.

[11] S. Vedhanayaki and V. Indragandhi, "Certain investigation and implementation of Coulomb counting based unscented Kalman filter for state of charge estimation of lithium-ion batteries used in electric vehicle application," *Int. J. Thermofluids*, vol. 18, May 2023, Art. no. 100335.

[12] K. Qian and X. Liu, "Hybrid optimization strategy for lithium-ion battery's state of charge/health using joint of dual Kalman filter and modified sine-cosine algorithm," *J. Energy Storage*, vol. 44, Dec. 2021, Art. no. 103319.

[13] H. Ben Sassi, F. Errahimi, N. Es-Sbai, and C. Alaoui, "Comparative study of ANN/KF for on-board SOC estimation for vehicular applications," *J. Energy Storage*, vol. 25, Oct. 2019, Art. no. 100822.

[14] V. Selvaraj and I. Vairavasundaram, "A comprehensive review of state of charge estimation in lithium-ion batteries used in electric vehicles," *J. Energy Storage*, vol. 72, Nov. 2023, Art. no. 108777.

[15] J. Tian, C. Chen, W. Shen, F. Sun, and R. Xiong, "Deep learning framework for lithium-ion battery state of charge estimation: Recent advances and future perspectives," *Energy Storage Mater.*, vol. 61, Aug. 2023, Art. no. 102883.

[16] E. Chemali, P. J. Kollmeyer, M. Preindl, R. Ahmed, and A. Emadi, "Long short-term memory networks for accurate state-of-charge estimation of Li-ion batteries," *IEEE Trans. Ind. Electron.*, vol. 65, no. 8, pp. 6730–6739, Aug. 2018.

[17] D. Liu, L. Li, Y. Song, L. Wu, and Y. Peng, "Hybrid state of charge estimation for lithium-ion battery under dynamic operating conditions," *Int. J. Elect. Power Energy Syst.*, vol. 110, pp. 48–61, Sep. 2019.

[18] B. Xiao, Y. Liu, and B. Xiao, "Accurate state-of-charge estimation approach for lithium-ion batteries by gated recurrent unit with ensemble optimizer," *IEEE Access*, vol. 7, pp. 54192–54202, 2019.

[19] P. Eleftheriadis, A. Dolara, and S. Leva, "An overview of data-driven methods for the online state of charge estimation," in *Proc. IEEE Int. Conf. Environ. Electr. Eng. IEEE Ind. Commercial Power Syst. Eur. (EEEIC/I&CPS Europe)*, Jun. 2022, pp. 1–6.

[20] Z. Huang, F. Yang, F. Xu, X. Song, and K.-L. Tsui, "Convolutional gated recurrent unit–recurrent neural network for state-of-charge estimation of lithium-ion batteries," *IEEE Access*, vol. 7, pp. 93139–93149, 2019.

[21] Z. Yi and P. H. Bauer, "Effects of environmental factors on electric vehicle energy consumption: A sensitivity analysis," *IET Electr. Syst. Transp.*, vol. 7, no. 1, pp. 3–13, Mar. 2017.

[22] F. Mohammadi, "Lithium-ion battery state-of-charge estimation based on an improved Coulomb-counting algorithm and uncertainty evaluation," *J. Energy Storage*, vol. 48, Apr. 2022, Art. no. 104061.

[23] J. Meng, M. Ricco, G. Luo, M. Swierczynski, D.-I. Stroe, A.-I. Stroe, and R. Teodorescu, "An overview and comparison of online implementable SOC estimation methods for lithium-ion battery," *IEEE Trans. Ind. Appl.*, vol. 54, no. 2, pp. 1583–1591, Mar. 2018.

[24] K. Qian, X. Liu, Y. Wang, X. Yu, and B. Huang, "Modified dual extended Kalman filters for SOC estimation and online parameter identification of lithium-ion battery via modified gray wolf optimizer," *Proc. Inst. Mech. Eng., D, J. Automobile Eng.*, vol. 236, no. 8, pp. 1761–1774, 2022.

[25] F. Yang, S. Zhang, W. Li, and Q. Miao, "State-of-charge estimation of lithium-ion batteries using LSTM and UKF," *Energy*, vol. 201, Jun. 2020, Art. no. 117664.

[26] C. Li, F. Xiao, and Y. Fan, "An approach to state of charge estimation of lithium-ion batteries based on recurrent neural networks with gated recurrent unit," *Energies*, vol. 12, no. 9, p. 1592, Apr. 2019.

[27] P. Eleftheriadis, S. Leva, and E. Ogliari, "Bayesian hyperparameter optimization of stacked bidirectional long short-term memory neural network for the state of charge estimation," *Sustain. Energy, Grids Netw.*, vol. 36, Dec. 2023, Art. no. 101160.

[28] C. Menos-Aikateriniadis, I. Lamprinos, and P. S. Georgilakis, "Particle swarm optimization in residential demand-side management: A review on scheduling and control algorithms for demand response provision," *Energies*, vol. 15, no. 6, p. 2211, Mar. 2022.

[29] L. Chen, Z. Wang, Z. Lü, J. Li, B. Ji, H. Wei, and H. Pan, "A novel state-of-charge estimation method of lithium-ion batteries combining the grey model and genetic algorithms," *IEEE Trans. Power Electron.*, vol. 33, no. 10, pp. 8797–8807, Oct. 2018.

[30] M. Jiao, D. Wang, and J. Qiu, "A GRU-RNN based momentum optimized algorithm for SOC estimation," *J. Power Sour.*, vol. 459, May 2020, Art. no. 228051.

[31] Z. Zhang, Z. Dong, H. Lin, Z. He, M. Wang, Y. He, X. Gao, and M. Gao, "An improved bidirectional gated recurrent unit method for accurate state-of-charge estimation," *IEEE Access*, vol. 9, pp. 11252–11263, 2021.

[32] W. He, N. Williard, C. Chen, and M. Pecht, "State of charge estimation for Li-ion batteries using neural network modeling and unscented Kalman filter-based error cancellation," *Int. J. Elect. Power Energy Syst.*, vol. 62, pp. 783–791, Nov. 2014.

[33] E. Chemali, P. J. Kollmeyer, M. Preindl, and A. Emadi, "State-of-charge estimation of Li-ion batteries using deep neural networks: A machine learning approach," *J. Power Sources*, vol. 400, pp. 242–255, Oct. 2018.

[34] D. N. T. How, M. A. Hannan, M. S. H. Lipu, K. S. M. Sahari, P. J. Ker, and K. M. Muttaqi, "State-of-charge estimation of Li-ion battery in electric vehicles: A deep neural network approach," *IEEE Trans. Ind. Appl.*, vol. 56, no. 5, pp. 5565–5574, Sep. 2020.

[35] Y. Tian, R. Lai, X. Li, L. Xiang, and J. Tian, "A combined method for state-of-charge estimation for lithium-ion batteries using a long short-term memory network and an adaptive cubature Kalman filter," *Appl. Energy*, vol. 265, May 2020, Art. no. 114789.

[36] C. Bian, H. He, and S. Yang, "Stacked bidirectional long short-term memory networks for state-of-charge estimation of lithium-ion batteries," *Energy*, vol. 191, Jan. 2020, Art. no. 116538.

[37] S. Elmi and K.-L. Tan, "DeepFEC: Energy consumption prediction under real-world driving conditions for smart cities," in *Proc. Web Conf.*, 2021, pp. 1880–1890.

[38] A. Gomaa, M. M. Abdelwahab, M. Abo-Zahhad, T. Minematsu, and R.-I. Taniguchi, "Robust vehicle detection and counting algorithm employing a convolution neural network and optical flow," *Sensors*, vol. 19, no. 20, p. 4588, Oct. 2019.

[39] A. Gomaa, T. Minematsu, M. M. Abdelwahab, M. Abo-Zahhad, and R. Taniguchi, "Faster CNN-based vehicle detection and counting strategy for fixed camera scenes," *Multimedia Tools Appl.*, vol. 81, no. 18, pp. 25443–25471, 2022.

[40] Y. Chang, Z. Tu, W. Xie, B. Luo, S. Zhang, H. Sui, and J. Yuan, "Video anomaly detection with spatio-temporal dissociation," *Pattern Recognit.*, vol. 122, Feb. 2022, Art. no. 108213.

[41] A. Gomaa, M. M. Abdelwahab, and M. Abo-Zahhad, "Efficient vehicle detection and tracking strategy in aerial videos by employing morphological operations and feature points motion analysis," *Multimedia Tools Appl.*, vol. 79, no. 35, pp. 26023–26043, 2020.

SELVARAJ VEDHANAYAKI received the B.E. degree in electrical and electronics engineering from Anna University and the M.E. degree in power systems from the Government College of Technology, Coimbatore. She is currently a Research Scholar with the School of Electrical Engineering, VIT University, Vellore, Tamil Nadu. Her research interests include power converters, artificial intelligence, and electric vehicle.

VAIRAVASUNDARAM INDRAGANDHI received the B.E. degree in electrical and electronics engineering from Bharathidasan University, in 2004, the M.E. degree in power electronics and drives from Anna University, Chennai, India, and the Doctor of Philosophy degree. She accomplished the thesis for her Ph.D. entitled "Analysis and Modeling of Multi-Port DC-DC Boost Converter for Hybrid Power Generation System" with Anna University. She is currently a Professor with the School of Electrical Engineering, VIT University, Vellore, Tamil Nadu. She has been engaged in research work for the past 15 years in the area of power electronics, drives and renewable energy systems. Her research interests include power converters, artificial intelligence, and power quality. She was awarded the Gold Medal for the achievement of the university's first rank.